ChemComm

COMMUNICATION

View Article Online
View Journal | View Issue

Cite this: *Chem. Commun.*, 2023, 59, 4483

Received 4th December 2022,
Accepted 13th March 2023

DOI: 10.1039/d2cc06597e

rsc.li/chemcomm

Single nanowire-based fluorescence lifetime thermometer for simultaneous measurement of intra- and extra-cellular temperatures†

Yuan Wang,[ab] Qiaowen Zhao,[ab] Sen Liang,[ab] Mingliang Mei,[ab] Guangwei She,[a] Wensheng Shi*[ab] and Lixuan Mu*[a]

A silicon nanowire-based fluorescence lifetime thermometer (NWFLT) was fabricated for the simultaneous measurement of intra- and extra-cellular temperatures. Using the NWFLT, an obvious heterogeneity of the temperature was found along the longitude direction of the NWFLT, especially between the inside and outside of the cell.

A temperature difference between the individual cells and the extracellular environment broadly exists, which is extensively connected to basic cellular metabolism, cellular pathways, gene expression, and so on.[1–4] Thorough research on temperature differences is also beneficial to understanding the pathogenesis and treatment of diseases.[5,6] In reality, determining the temperature difference during the simultaneous measurement of the intra- and extra-cellular temperatures is postulated.[7] Among the many methods used to detect the temperature of the individual cell, fluorescent strategies have attracted much research interest due to the significant advantages of high sensitivity, rapid testing, non-contact detection mode, and so on.[8–12] However, only a few research studies have realized the simultaneous detection of intra- and extra-cellular temperatures using micro sized materials.[7,13,14] Some researchers have developed fluorescence lifetime-based thermometers for cells, by which the interference from the probe concentration, fluctuation of the light source, inconsistent permeability of the fluorophore and photobleaching could be eliminated.[15–18] However, the low spatial resolution resulting from the drift of the nanomaterial still remained during the measurement, and the thermometer could not detect the extra-cellular temperature.

Herein, using the advantages of the fluorescence lifetime (FL) as a signal to respond to the temperature, and the nanowires as a block to build the thermometer, we anchored Rhodamine B (RhB) onto the surface of silicon nanowires (SiNWs) and constructed a SiNWs-based fluorescence lifetime thermometer (NWFLT) for use in cells (Scheme 1). The SiNWs have excellent biocompatibility and low thermal conductivity and have been widely used as the supporting section in sensors.[19–21] With the rise of the temperature, the rate of the non-radiative transition of the RhB in the excited states increased,[22] and as a result, the FL of the RhB would decrease distinctly. Employing the sensitive dependence of the FL of the NWFLT on the temperature, we can precisely determine the temperature by measuring the FL. Moreover, the configuration of anchoring the RhB onto the SiNWs can efficiently suppress the continual drift of the zero dimensional nanosized thermometer and greatly enhance its spatial resolution during the measurement.[23–25] Using the NWFLT assisted by FL imaging microscopy (FLIM), we simultaneously obtained the intra- and extra-cellular temperatures with a high spatial resolution. The method developed in this work facilitates the investigation of the heat exchange between the individual cell and the extra-cellular environment, which is postulated for exploring numerous cellular physiological processes.

Silver (Ag^+)-assisted chemical etching was used to fabricate the SiNWs according to methods in previous reports.[26,27] The length of the SiNWs was about 60 μm (Fig. S1a, ESI†) and the diameters of the SiNWs ranged from about 100 nm to 500 nm (Fig. S1b, ESI†). So a small diameter has little influence on the cells that were penetrated by the single SiNW.[25] The SiNWs were annealed at 900 °C for various times to increase the thickness of

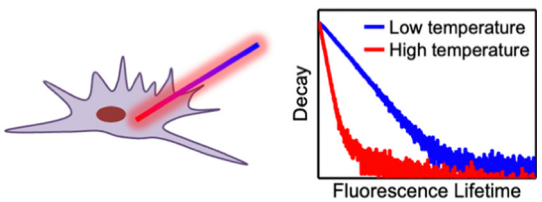

Scheme 1 (a) Schematic diagram of the NWFLT for simultaneous measurement of intra- and extra-cellular temperatures by FLIM.

[a] *Key Laboratory of Photochemical Conversion and Optoelectronic Materials, Technical Institute of Physics and Chemistry, Chinese Academy of Sciences, Beijing 100190, China. E-mail: mulixuan@mail.ipc.ac.cn, Shiws@mail.ipc.ac.cn*

[b] *University of Chinese Academy of Sciences, Beijing 100049, China*

† Electronic supplementary information (ESI) available. See DOI: https://doi.org/10.1039/d2cc06597e

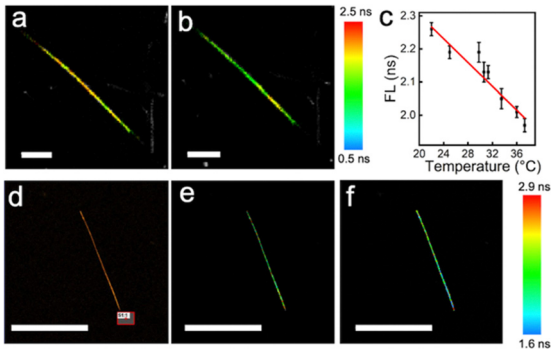

Fig. 1 The FLIM images of the NWFLT at 25.0 °C (a) and 36.0 °C (b), the FL of the single NWFLT *vs.* temperature (c). (d) The fluorescence image of the single NWFLT, the red rectangular area (S1 : 1) was stimulated with a 561 nm laser. The FLIM images of the NWFLT before (e) and after (f) stimulation with a 561 nm laser for 10 min. The scale bars in (a) and (b) are 10 μm, and in (d), (e) and (f) are 60 μm.

the SiO_2 on the SiNWs (Fig. S2, ESI†). Then, the surface of the SiNWs wrapped by the SiO_2 was decorated with RhB by the connection of the secondary ammonia reagent.[28] The RhB-modified SiNWs exhibited a bright fluorescence (Fig. S3a, ESI†), and the results of the fluorescence spectroscopy of the RhB-modified SiNW are consistent with those of the RhB in the solution (Fig. S3b, ESI†), indicating the successful modification of the RhB on the SiNWs. Thus, the RhB-modified SiNWs with SiO_2 were used as the NWFLT in the subsequent experiments.

The dependence of the FL of the NWFLT on the temperatures was investigated using FLIM, the temperature of which was regulated with the living-cell workstation (LCW). As shown in Fig. 1a and b, when the system was fixed at 25.0 °C or 36.0 °C, the NWFLT could be recognized clearly by its uniform color distribution in the FLIM image at a certain temperature. The obvious change of the color from amber to green indicated the evident decrease of the FL of the NWFLT as the system temperature increased from 25.0 °C to 36 °C. The FLIM images with striking color changes could be utilized as a remarkable approach to monitor temperature alterations. Averaging the FL of the NWFLT, it was found that the mean FL of the NWFLT decreased gradually from 2.26 ns to 1.97 ns as the temperature increased from about 22.0 °C to 37.3 °C (Fig. 1c). According to the reported method,[29] the relative sensitivity of the NWFLT to the temperature could be calculated to be 1.4% $°C^{-1}$, which is comparable with that of other reported FLTs.[30,31] The high relative sensitivity of the NWFLT can be attributed to the remarkable sensitivity of the RhB that was on the surface of the NWFLT (the relative sensitivities of the RhB at different temperatures are shown in the Fig. S4, ESI†).

To reveal the spatial resolution of the NWFLT, commercial gold nanorods (80 nm in length and 20 nm in diameter) were placed on the bottom of the confocal observation dish to produce a spot heat source. When the area (S1 : 1) marked by the red box in the Fig. 1d was irradiated by the 561 nm laser, its temperature was elevated due to the efficient photothermal effect of the gold nanorods. As the distribution of the temperature gradient was from the S1 : 1 to the surroundings, the color of the NWFLT close to the S1 : 1 changed to blue after the irradiation (from 2.48 ns to 1.81 ns), meaning that an obvious increase in the temperature occurred, whereas that of the far end of the NWFLT exhibited little change as shown in Fig. 1e and f. These results demonstrated that the temperature distribution in a tiny area could be easily distinguished by the NWFLT with a high spatial resolution.

In order to assess the anti-interference of the NWFLT, Na^+, Ca^{2+}, K^+, Mg^{2+} and bovine serum albumin (BSA), were added to the test solution. The FL of the NWFLT showed little change from the interference of the previous agents (Fig. S5a, ESI†). Moreover, the FL of the NWFLT in the solutions with a series of pH from 4.8 to 8.8, also maintained a constant value (Fig. S5b, ESI†). These results showed that the NWFLT had excellent anti-interference ability, which endows the NWFLT with the capability to work in an intricate cellular environment. Furthermore, when compared with a commercial mitochondrial dye (MitoView Blue), the NWFLT also exhibits outstanding photostability (Fig. S6, ESI†), which enable it to be suitable for use in long-term observation.

The NWFLT was dispersed into PBS solution in a cell culture dish, and then the seeded L929 cells (mouse fibroblast cells) were co-incubated with the NWFLT for 24 h. Subsequently, the L929 cells were stained with the commercial cell dyes. The fluorescence intensity images (Fig. 2) and the Z-series scanning video (Video SI, ESI†) showed that the NWFLT has been incubated into the cell.[13] Accordingly, observing the merged image of the co-incubated NWFLT and L929 cells (Fig. 2c), we found that part of the NWFLT has been incubated into the L929 cell, while the remainder of the NWFLT was still outside the cell, The clear location relationship between the cell and NWFLT provides a platform for investigating the temperature of the cell with the NWFLT.

The effect of the surrounding temperature on the cellular temperature was explored using the NWFLT. After the NWFLT was incubated into the L929 cell, the cell culture was heated by the LCW attached to the FLIM. The cells in the FLIM images (Fig. 3a and b) are outlined by the yellow dotted line according to the differential interference contrast microscopy (DIC) image shown in Fig. 3c. As the surrounding temperature increased from 27.0 °C to 38.0 °C, the FL of the NWFLT from point E_1 to C_1 changed from 2.13 ns to 2.05 ns, meanwhile, that from point C_1 to E_2 changed from 2.09 ns to 2.05 ns (Fig. 3a and b),

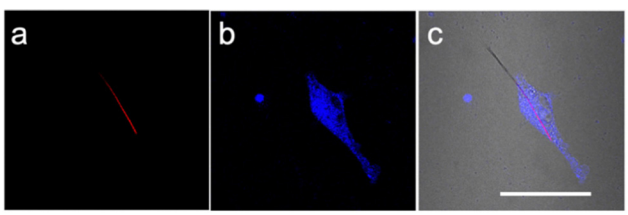

Fig. 2 (a) The fluorescence image of the single NWFLT incubated with L929 cells. (b) The NWFLT and a L929 cell stained with cytoplasmic blue dye. (c) The merged image of (a) and (b) to give a bright field image. The scale bar is 50 μm.

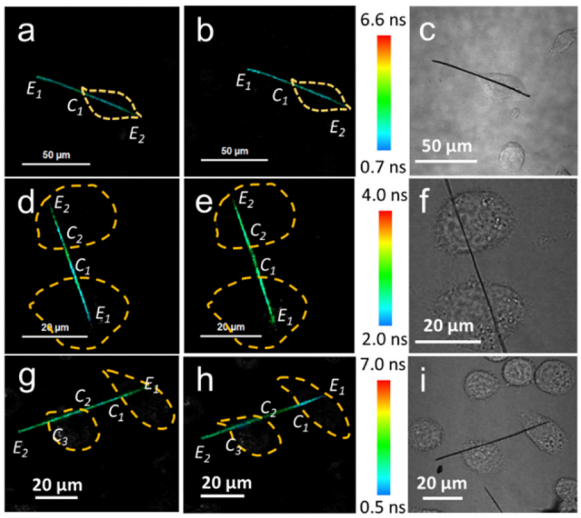

Fig. 3 The FLIM images of the NWFLT incubated with a single cell at different temperatures (a) 27.0 °C and (b) 38.0 °C). (c), (f) and (i) are the DIC images. The FLIM images of the NWFLT with (d) and without (e) 10 mM Ca^{2+}, and the FLIM images of the NWFLT with (g) and without (h) 10 μM CCCP, and the cells are noted by the yellow dotted line. The endpoints of the NWFLT are marked as point E, and the contact positions of the cell membrane with NWFLT are marked as C.

meaning that the intracellular temperature increased slightly with the obvious elevation of the surrounding temperature. These results indicate that to a certain extent, the cell could resist the influence of the surrounding temperature.

It has been reported that Ca^{2+} and carbonyl cyanide *m*-chlorophenyl hydrazone (CCCP) could decrease and increase the cellular temperatures, respectively.[7,28,32–36] The NWFLT was used to assess the effect of Ca^{2+} and CCCP on the cellular temperature. The mean FL of the NWFLT in the cell (from E_1 to C_1, Fig. 3d) is about 1.54 ns. After Ca^{2+} (10 μL, 10 mM) was added to the cell culture for 30 min, the mean FL of the NWFLT from E_1 to C_1 increased to 1.79 ns, whereas, the color of the NWFLT from E_1 to C_1 changed from blue to green as can be seen from Fig. 3d and e. Whereas the mean FL of the NWFLT out of the cell (from C_1 to C_2) simultaneously exhibited little change from 1.89 ns to 1.86 ns, before and after the addition of Ca^{2+}. The increase of FL means that the Ca^{2+} induced a decrease in cellular temperature. Moreover, the temperature of the other cell is stimulated by the Ca^{2+} synchronously, and attached to the same NWFLT and the temperature also decreased according to the color variation of the NWFLT from C_2 to E_2 shown in Fig. 3d and e. In contrast to the Ca^{2+}, CCCP can uncouple the oxidative phosphorylation, and by which the cellular temperature increases.[7,28] Observing the FLIM images before (Fig. 3g) and after (Fig. 3h) adding 10 μL of the CCCP (10 μM), it can be determined that the mean FL of the NWFLT in the cell (E_1 to C_1) decreased from 1.80 ns to 1.73 ns, whereas the color of the NWFLT varied from cyan to turquoise, indicating that the cellular temperature was apparently elevated by the CCCP. Meanwhile, the color of the NWFLT out of the cell (C_1 to C_2 and C_3 to E_2) exhibited little change. Observing the other cell attached to the same NWFLT, we found that the color of the NWFLT (C_2 to C_3) changed slightly (the FL changed from 1.80 ns to 1.76 ns), and this represented the difference between the temperature alteration of the two cells by the CCCP, and this may be related to cellular heterogeneity.[2] Furthermore, from observing the cells in Fig. 3a, d and g, we find that the mean FL of the NWFLT in the cells are lower than that outside the cell, revealing that the intra-cellular temperature was higher than the extra-cellular temperature before the stimulations. More statistical analysis can be found in Tables S1–S3 (ESI†). All these results demonstrate that the single NWFLT can not only simultaneously measure the intra- and extra-cellular temperature, but can also detect the temperatures of several cells concurrently.

The dependence of the cellular temperature on apoptosis was not clear. When the apoptosis is occurring, the cell shows shrinkage, blebbing, and produces apoptotic bodies.[37] Therefore, the morphology of the cell would change a lot.[38] If the fluorescence intensity was employed to detect the temperature of the cell, the obvious transformation of the cell morphologies would cause a signal fluctuation. As a result, it would be difficult to accurately determine the intra-cellular temperature by the fluorescence intensity during apoptosis. Here, the temperature changes of the cell during apoptosis were observed by the NWFLT. A live/dead cell (L929) assay was conducted to prove the excellent biocompatibility of the silicon nanowires (Fig. S7, ESI†). The L929 cells were co-incubated with the NWFLT. A single NWFLT was inserted into the individual cell (Fig. 4). Enough cisplatin (125 μM) was added into the cell culture dish to induce apoptosis (Fig. S8, ESI†). After 2 min, the cell exhibited blebbing, which indicated the start of apoptosis. According to the FLIM images in Fig. 4, from 0 min to 90 min, the FL of the NWFLT in the cell increased from 1.58 ns to 2.66 ns, indicating the decrease of the cellular temperature during the apoptosis. After 90 min, the cells were dead, and the temperature of the dead cell was lower than that of the live cell. The decrease in cellular temperature may originate from the cessation of the intra-cellular physiological processes due to apoptosis. Moreover, it was simultaneously observed that the temperature of the NWFLT out of the cell also decreased slightly

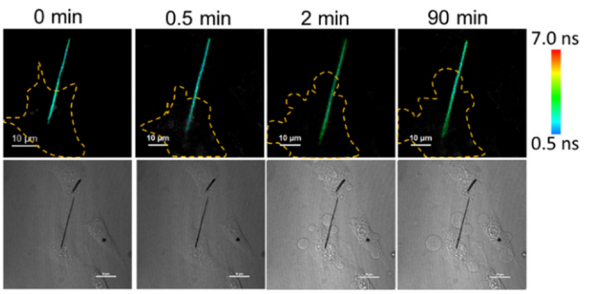

Fig. 4 The FL images of the NWFLT incubated with a single cell after adding 125 μM cisplatin for various times as shown in the top row. The DIC images of the NWFLT and the single cell at various times are shown in the bottom row. The cells are noted by the yellow dotted line, and the scale bars of the DIC images are 20 μm.

during the apoptosis, which may be dominated by the heat diffusion from the environment to the cell. These results indicated that the NWFLT can be anticipated to simultaneously measure the changes of the intra- and extra-cellular temperatures in more physiological processes.

In conclusion, a NWFLT was fabricated based on the FL of the RhB and a silicon nanowire for simultaneously measuring the change of intra- and extra-cellular temperatures. A high relative sensitivity of 1.4% $^{\circ}C^{-1}$ was achieved by the NWFLT. Due to the high spatial resolution of the NWFLT, the simultaneous measurement of the intra- and extra-cellular temperatures can be realized. Moreover, the dependence of the intra- and extra-cellular temperatures on the stimulation of the CCCP and Ca^{2+} were successfully detected by the NWFLT. Meanwhile, the temperature decrease of the cell during apoptosis was determined by the NWFLT. The strategy developed in this work for simultaneously exploring the intra- and extra-cellular temperatures at a high spatial resolution is promising for potential applications to investigate the temperature-related cellular physiological processes.

This work was supported by the National Key R&D Program of China (Grant No. 2017YFE0196400 and 2022YFB3803600), the National Natural Science Foundation of China (NSFC, Grant No. 52172107 and 21975269).

Conflicts of interest

There are no conflicts to declare.

Notes and references

1 T. D. Vreugdenburg, C. D. Willis, L. Mundy and J. E. Hiller, *Breast Cancer Res. Treat.*, 2013, **137**, 665–676.
2 P. Song, H. Gao, Z. Gao, J. Liu, R. Zhang, B. Kang, J.-J. Xu and H.-Y. Chen, *Chemistry*, 2021, 7, 1569–1587.
3 Y. Kamei, M. Suzuki, K. Watanabe, K. Fujimori, T. Kawasaki, T. Deguchi, Y. Yoneda, T. Todo, S. Takagi, T. Funatsu and S. Yuba, *Nat. Methods*, 2009, **6**, 79–81.
4 N. C. Wegner, O. E. Snodgrass, H. Dewar and J. R. Hyde, *Science*, 2015, **348**, 786–789.
5 Y. Houdas and E. F. J. Ring, *Human Body Temperature Its Measurement and Regulation*, Springer, Boston, MA, 1982.
6 K. Bowler, H. Laudien and I. Laudien, *J. Therm. Biol.*, 1983, **8**, 426–430.
7 K. Oyama, M. Gotoh, Y. Hosaka, T. G. Oyama, A. Kubonoya, Y. Suzuki, T. Arai, S. Tsukamoto, Y. Kawamura, H. Itoh, S. A. Shintani, T. Yamazawa, M. Taguchi, S. Ishiwata and N. Fukuda, *J. Gen. Physiol.*, 2020, **152**, 201912469.
8 T.-R. Xie, C.-F. Liu and J.-S. Kang, *Biophys. Rep.*, 2017, **3**, 85–91.
9 B. del Rosal, D. Ruiz, I. Chaves-Coira, B. H. Juárez, L. Monge, G. Hong, N. Fernández and D. Jaque, *Adv. Funct. Mater.*, 2018, **28**, 1806088.
10 X. D. Wang, O. S. Wolfbeis and R. J. Meier, *Chem. Soc. Rev.*, 2013, **42**, 7834–7869.
11 E. Zhang, S. Xiang and A. Fu, *J. Nanosci. Nanotechnol.*, 2016, **16**, 6597–6610.
12 F. Yuan, L. Ding, Y. Li, X. Li, L. Fan, S. Zhou, D. Fang and S. Yang, *Nanoscale*, 2015, **7**, 11727–11733.
13 C. Bu, L. Mu, X. Cao, M. Chen, G. She and W. Shi, *ACS Appl. Mater. Interfaces*, 2018, **10**, 33416–33422.
14 Z. Gong, T. Wu, X. Chen, J. Guo, Y. Zhang and Y. Li, *Nano Lett.*, 2021, **21**, 1469–1476.
15 C. Gota, S. Uchiyama, T. Yoshihara, S. Tobita and T. Ohwada, *J. Phys. Chem. B*, 2008, **112**, 2829–2836.
16 T. Bai and N. Gu, *Small*, 2016, **12**, 4590–4610.
17 K. Suhling, L. M. Hirvonen, J. A. Levitt, P.-H. Chung, C. Tregidgo, A. Le Marois, D. A. Rusakov, K. Zheng, S. Ameer-Beg, S. Poland, S. Coelho, R. Henderson and N. Krstajic, *Med. Photonics*, 2015, **27**, 3–40.
18 H. Gao, C. Kam, T. Y. Chou, M. Y. Wu, X. Zhao and S. Chen, *Nanoscale Horiz.*, 2020, **5**, 488–494.
19 Z. Han and A. Fina, *Prog. Polym. Sci.*, 2011, **36**, 914–944.
20 D. Li, Y. Wu, P. Kim, L. Shi, P. Yang and A. Majumdar, *Appl. Phys. Lett.*, 2003, **83**, 2934–2936.
21 X. Cao, L. Mu, M. Chen and G. She, *Appl. Surf. Sci.*, 2018, **441**, 388–393.
22 J. R. Lakowicz, *Principles of Fluorescence Spectroscopy*, Mary land, Baltimore, USA, 3rd edn, 2006.
23 B. Tian and C. M. Lieber, *Chem. Rev.*, 2019, **119**, 9136–9152.
24 A. Tay and N. Melosh, *Acc. Chem. Res.*, 2019, **52**, 2462–2471.
25 X. Cao, L. Mu, M. Chen, C. Bu, S. Liang, G. She and W. Shi, *Adv. BioSyst.*, 2018, **2**, 1–7.
26 K. Peng, A. Lu, R. Zhang and S.-T. Lee, *Adv. Funct. Mater.*, 2008, **18**, 3026–3035.
27 K. Q. Peng, J. J. Hu, Y. J. Yan, Y. Wu, H. Fang, Y. Xu, S. T. Lee and J. Zhu, *Adv. Funct. Mater.*, 2006, **16**, 387–394.
28 Z. L. Huang, N. Li, X. F. Zhang, C. Wang and Y. Xiao, *Anal. Chem.*, 2018, **90**, 13953–13959.
29 S. Liang, Y. Wang, X. Wu, M. Chen, L. Mu, G. She and W. Shi, *Chem. Commun.*, 2019, **55**, 3509–3512.
30 H. Itoh, S. Arai, T. Sudhaharan, S. C. Lee, Y. T. Chang, S. Ishiwata, M. Suzuki and E. B. Lane, *Chem. Commun.*, 2016, **52**, 4458–4461.
31 O. S. Wolfbeis, *Anal. Chem.*, 2006, **78**, 3859–3874.
32 E. K. Ainscow and G. A. Rutter, *Diabetes*, 2002, **51**(Suppl 1), S162–S170.
33 D. Jaque, B. D. Rosal, E. M. Rodriguez, L. M. Maestro, P. Haro-Gonzalez and J. G. Sole, *Nanomedicine*, 2014, **9**, 1047–1062.
34 W. Qiang, H. Hu, L. Sun, H. Li and D. Xu, *Anal. Chem.*, 2015, **87**, 12190–12196.
35 J. Qiao, C. Chen, D. Shangguan, X. Mu, S. Wang, L. Jiang and L. Qi, *Anal. Chem.*, 2018, **90**, 12553–12558.
36 J. Qiao, Y. H. Hwang, D. P. Kim and L. Qi, *Anal. Chem.*, 2020, **92**, 8579–8583.
37 J. Tian, X. Zeng, X. Xie, S. Han, O. W. Liew, Y. T. Chen, L. Wang and X. Liu, *J. Am. Chem. Soc.*, 2015, **137**, 6550–6558.
38 T. Zhang, Y. Li, Z. Zheng, R. Ye, Y. Zhang, R. T. K. Kwok, J. W. Y. Lam and B. Z. Tang, *J. Am. Chem. Soc.*, 2019, **141**, 5612–5616.

